International Journal of Thermal Sciences 49 (2010) 454–462

Contents lists available at ScienceDirect

International Journal of Thermal Sciences

journal homepage: www.elsevier.com/locate/ijts

Conceptual optimization of a rotary heat exchanger with a porous core

Jonathan Dallaire [a], Louis Gosselin [a,*], Alexandre K. da Silva [b]

[a] Département de génie mécanique, Université Laval, Québec City, Québec, Canada G1V 0A6
[b] Department of Mechanical Engineering, University of Texas at Austin, Austin, TX 78712, USA

ARTICLE INFO

Article history:
Received 19 May 2009
Received in revised form
27 July 2009
Accepted 30 July 2009

Keywords:
Rotary heat exchanger
Optimal design
Maximum heat transfer
Heat storage

ABSTRACT

The present article numerically optimizes the thermal performance of a rotary heat exchanger (RHEx) where its internal structure is modeled as a porous medium. The objective is to maximize the RHEx's heat transfer rate per unit of frontal surface area (q''). The flow velocity through the porous matrix respects Darcy's law. Two thermal conditions between the solid matrix and the fluid are considered: (i) local thermal equilibrium – LTE and (ii), non-local thermal equilibrium – NLTE. The numerical calculations, which are implemented using a finite volume formulation, allow us to optimize two design variables, the length L of the heat exchanger and the porosity φ. The numerical results show that the figure of merit is substantially affected by both design variables and that optimal values of L and φ can be obtained. The numerical experiments also show that the optimum porosity is not a function of the pressure difference driving the flow across the RHEx. The study ends by addressing the effects of the porosity distribution and differential periods between the hot and cold sides of RHEx on the figure of merit. The numerical results are supported by a scale analysis.

1. Introduction

Different types of heat transfer devices exist aiming to satisfy a hungry and diverse market. While ranging broadly from constructive and operational standpoints, heat exchangers – HEx have been grouped according to certain key features. Shah and Sekulic [1] present classifications of HEx based on several features: geometry, flow direction, number of different working fluids, etc. Furthermore, several techniques were developed aiming to facilitate the selection and design process of various heat exchanger configurations; good examples are the "number of transfer units" – NTU and the "log mean temperature difference" – LMTD methods [2].

Following the classification scheme previously discussed, the heat exchanger under consideration in the present article could be categorized as a counter-flow, porous-based rotational device or simply a rotary heat exchanger (RHEx). These devices, which are particularly suitable for gas-to-gas energy recovery, were considered by the literature numerous times while addressing, for example, economical aspects [3–5], conductive aspects through the internal structure [6–9], heat recovery applications [10–12], angular speed effects [13], leakage [14,15] and thermal issues [16–19].

In the present paper, we portray fundamental RHEx optimization opportunities. We demonstrate these opportunities with a numerical model of rotary heat exchanger. The hot and cold sides of the heat exchanger are subjected to independent pressure drops and different temperature levels. The objective is to maximize the heat transfer rate per unit of area of the RHEx under two thermal conditions between the solid matrix and fluid: (a) local thermal equilibrium and (ii), non-local thermal equilibrium. The numerical results are validated by an extensive scale analysis. The fundamental question of how to distribute the solid matrix and fluid flow is addressed.

2. Simplified model of heat wheel

The modeling begins by considering that the internal structure of the rotary heat exchanger (RHEx) can be represented by a porous structure as detailed in Fig. 1. Next, assuming that the solid and fluid composing the porous structure are in local thermal equilibrium and neglecting conduction heat transfer within the porous structure (these assumptions will be relaxed later) [20–22], the conservation of energy states that

$$\sigma\frac{\partial T}{\partial t}+u\frac{\partial T}{\partial x}=0 \tag{1}$$

where $\sigma=\phi+(1-\phi)(\rho c)_s/(\rho c)_f$ represents the dimensionless averaged volumetric heat capacity which depends on the porosity φ [23]. The following boundary conditions apply:

* Corresponding author. Tel.: +1 418 656 7829; fax: +1 418 656 7415.
E-mail address: louis.gosselin@gmc.ulaval.ca (L. Gosselin).

1290-0729/$ – see front matter © 2009 Elsevier Masson SAS. All rights reserved.
doi:10.1016/j.ijthermalsci.2009.07.027

Nomenclature

a	heat transfer area per unit volume, m^2/m^3
A	shape parameter for porosity distribution
B	shape parameter for porosity distribution
Be	Bejan number
c	heat capacity, J/(kg K)
D	hydraulic diameter of the channel/sphere diameter, m
h	heat transfer coefficient, $W/(m^2 K)$
K	permeability, m^2
L	length, m
Nu	Nusselt number
Pr	Prandtl number
q'	heat flux, W/m^2
Q''	heat transfer per unit of area, J/m^2
Re	Reynolds number
t	time, s
T	temperature, K
u	velocity, m/s
x	Cartesian coordinate, m

Greek symbols

α	thermal diffusivity, m^2/s
ΔP	pressure drop, Pa
θ	angle, rad
μ	dynamic viscosity, kg/(m s)
ρ	density, kg/m^3
σ	dimensionless volumetric heat capacity
τ	half period, s
φ	porosity

Superscripts

$\sim$	dimensionless variables

Subscripts

C	cold fluid stream
f	fluid
H	hot fluid stream
opt	optimal value
s	solid

$$T(x = 0, 0 \le t \le \tau) = T_H \quad T(x = L, \tau \le t \le 2\tau)) = T_C \tag{2}$$

where τ represents half of the period. The lateral side of the RHEx is assumed adiabatic. One should notice that in the first half of the cycle, heat is transferred from a hot fluid at T_H to the internal porous structure of the RHEx, and in the second half, heat is transferred from the internal porous structure to a cold incoming stream at T_C. In this paper, we are interested in the periodic solution which occurs, when $T(t) = T(t + 2\tau)$, after repeating several cycles. The averaged velocity within the porous structure can be determined from Darcy's law [23]

$$u = \frac{K\Delta P}{\mu L} \tag{3}$$

where the permeability K depends on the internal structure of the porous medium. Two different porosity geometries have been investigated: a series of parallel channels and a packing of spheres. The permeability for a series of parallel channels can be written as [20]

$$K = \frac{\phi D^2}{32} \tag{4}$$

where D is the hydraulic diameter of the channels, whereas for a packing of spheres, the permeability is given by [24]

$$K = \frac{D^2\phi^3}{150(1-\phi)^2} \tag{5}$$

where D is the diameter of the spheres.

The amount of energy transferred from the warm airflow to the cold airflow was obtained by integrating over the spatial domain the variation of internal energy contained in the solid matrix during half of the cycle (in the periodic regime).

$$Q'' = \int_0^L (1-\phi)(\rho c)_s [T(x, t = 0) - T(x, t = \tau)]\mathrm{d}x \tag{6}$$

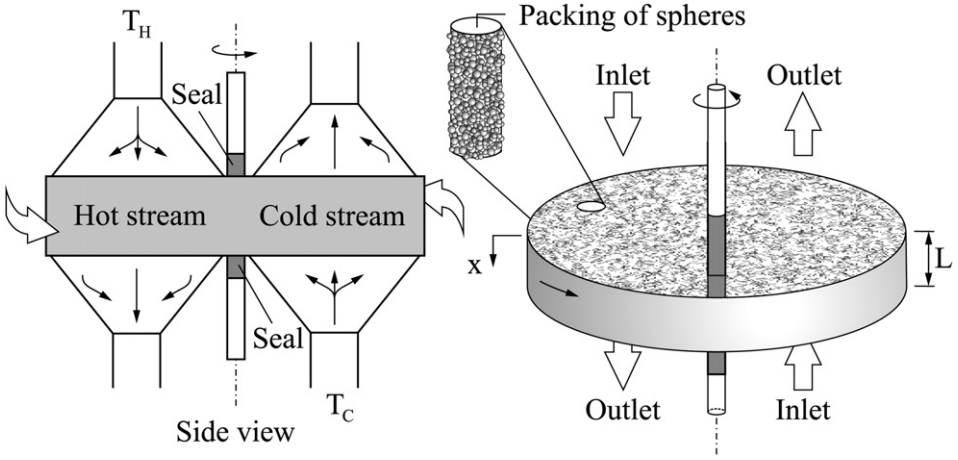

Fig. 1. Schematic representation of the heat exchanger.

Finally, one can define the figure of merit studied in this paper as the heat transfer rate per unit of heat wheel surface area after an entire cycle, which is achieved by dividing Eq. (6) by the period 2τ,

$$q'' = \frac{Q''}{2\tau} \tag{7}$$

Our objective is to maximize the heat transfer rate per unit of surface area, Eq. (7), by varying the porosity and the length of the system. The constitutive equations were non-dimensionalized using the following variables and parameters.

$$\tilde{T} = \frac{T-\overline{T}}{T_H - T_C} \quad \tilde{x} = \frac{x}{D} \quad \tilde{t},\tilde{\tau} = \frac{t,\tau}{D^2/\alpha} \quad \mathrm{Be} = \frac{\Delta P D^2}{\mu\alpha} \quad \tilde{L} = \frac{L}{D} \tag{8}$$

Eqs. (1), (6) and (7) become, for a series of parallel channels

$$\left[\phi + (1-\phi)\tilde{\rho}\tilde{c}\right]\frac{\partial\tilde{T}}{\partial\tilde{t}} + \frac{\phi}{32}\frac{\mathrm{Be}}{\tilde{L}}\frac{\partial\tilde{T}}{\partial\tilde{x}} = 0 \tag{9}$$

$$\tilde{Q}'' = \frac{Q''}{D(T_H - T_C)(\rho c)_f} = (1-\phi)\tilde{\rho}\tilde{c}\int_0^{\tilde{L}}\left[\tilde{T}_s\left(\tilde{x},\tilde{t}=0\right) - \tilde{T}_s\left(\tilde{x},\tilde{t}=\tilde{\tau}\right)\right]\mathrm{d}\tilde{x} \tag{10}$$

$$\tilde{q}'' = \frac{\tilde{Q}''}{2\tilde{\tau}} \tag{11}$$

where $\tilde{\rho}\tilde{c} = (\rho c)_s/(\rho c)_f$. For a packing of spheres, the following expression is used instead of Eq. (9):

$$\left[\phi + (1-\phi)\tilde{\rho}\tilde{c}\right]\frac{\partial\tilde{T}}{\partial\tilde{t}} + \frac{\phi^3}{(1-\phi)^2}\frac{\mathrm{Be}}{150\tilde{L}}\frac{\partial\tilde{T}}{\partial\tilde{x}} = 0 \tag{12}$$

It is important to emphasize that for the "leakage" to be negligible, it is necessary that the travel time of the fluid across the RHEx (i.e., from $x=0$ to $x=L$) be short compared to the period τ (i.e., $L/u \ll \tau$), which implies that

$$\tilde{\tau} \gg \frac{32\tilde{L}^2}{\phi\mathrm{Be}} \quad \tilde{\tau} \gg \frac{150\tilde{L}^2(1-\phi)^2}{\mathrm{Be}\phi^3} \tag{13}$$

for a series of parallel channels and a packing of spheres, respectively. Otherwise, the RHEx does not allow for heat transfer between the fluids and solid matrix.

3. Scale analysis and intersection of the asymptotes: local thermal equilibrium

In this section, we propose a scale analysis of the RHEx problem exposed in Section 2 in order to estimate its optimal features. The system is characterized by two design variables (i.e., $\tilde{L}$ and φ) and three parameters (i.e., $\tilde{\tau}$, Be and $\tilde{\rho}\tilde{c}$). We will present the order of magnitude of $\tilde{q}''$ in two limits: large $\tilde{L}$ and small $\tilde{L}$. Then, by intersecting these two asymptotes, we will be able to predict the optimal length and porosity. See [23,25] for more details on this method.

The first limiting case occurs when $\tilde{L}$ is small, which suggests that $t \ll \tau$. In this case, the temperature of the outflow stabilizes eventually to the inlet temperature. Starting from the beginning of a cycle, the moment when this happens scales as $t \sim \sigma L/u$. One may obtain this result by considering the order of magnitude of each term in Eq. (1). Assuming the temperature at the beginning of each cycle to be near T_C, the total heat transferred from the fluid to the porous structure may be estimated as

$$Q'' \sim (1-\phi)(\rho c)_s(T_H - T_C)L \tag{14}$$

Therefore, based on Eq. (10) and assuming $\sigma \sim (1-\phi)\tilde{\rho}\tilde{c}$ when $(\rho c)_s \gg (\rho c)_f$, the energy stored in the system and the average heat transfer rate are, for both porous structures considered

$$\tilde{Q}'' \sim \tilde{L}\sigma \quad \tilde{q}'' \sim \frac{\tilde{L}\sigma}{2\tilde{\tau}} \quad \left(\text{small } \tilde{L}\right) \tag{15}$$

For longer systems ($t \gg \tau$), the length thermally influenced by the inflow during the period τ is $x \sim \tau u/\sigma$. This corresponds to the second asymptote. Once again, this result is obtained by considering the order of magnitude of each term in Eq. (1). For such systems, the fluid temperature will stabilize to the temperature of the region of the porous structure unaffected by the flow. Therefore, the heat transferred may be approximated as

$$Q'' \sim u(\rho c)_f(T_H - T_C)\tau \tag{16}$$

Using Eq. (3) to express the fluid velocity in terms of ϕ and Be for a series of parallel channels and non-dimentionalizing with Eq. (10), the energy stored and average heat transfer rate are given by

$$\tilde{Q}'' \sim \frac{\phi}{32\tilde{L}}\mathrm{Be}\tilde{\tau} \quad \tilde{q}'' \sim \frac{\phi}{64\tilde{L}}\mathrm{Be} \quad \left(\text{large } \tilde{L}\right) \tag{17}$$

Intersecting these two asymptotes allow one to estimate the optimal length of the heat wheel and maximal heat transfer rate

$$\tilde{L}_{opt} \sim \left(\frac{\phi}{32(1-\phi)\tilde{\rho}\tilde{c}}\mathrm{Be}\tilde{\tau}\right)^{1/2} \quad \tilde{q}''_m \sim \left(\frac{\phi(1-\phi)\tilde{\rho}\tilde{c}}{128}\frac{\mathrm{Be}}{\tilde{\tau}}\right)^{1/2} \tag{18}$$

Differentiating Eq. (18) with respect to φ and equalling to zero yields

$$\phi_{opt} \sim 0.5 \quad \tilde{L}_{opt} \sim \left(\frac{1}{32\tilde{\rho}\tilde{c}}\mathrm{Be}\tilde{\tau}\right)^{1/2} \quad \tilde{q}''_{mm} \sim \left(\frac{\tilde{\rho}\tilde{c}}{512}\frac{\mathrm{Be}}{\tilde{\tau}}\right)^{1/2} \tag{19}$$

These results apply to the parallel channel model. Based on this scale analysis, the optimal porosity is independent on the governing parameters. The optimal length of the heat wheel increases with Be and $\tilde{\tau}$, and diminishes with the solid-to-fluid heat capacity ratio. Finally, the heat transfer rate is an increasing function of both Be and the solid-to-fluid heat capacity ratio, and a decreasing function of the period $\tilde{\tau}$. Again, it should be noted that it is not possible to decrease indefinitely the period, because the time of residence of the fluid within the matrix must be small compared to the period.

In a similar manner, one may find expressions for the optimal length and maximal heat transfer rate for a packing of spheres as a function of ϕ:

$$\tilde{L}_{opt} \sim \left(\frac{\phi^3}{150(1-\phi)^3\tilde{\rho}\tilde{c}}\mathrm{Be}\tilde{\tau}\right)^{1/2} \quad \tilde{q}''_m \sim \left(\frac{\tilde{\rho}\tilde{c}\phi^3}{600(1-\phi)}\frac{\mathrm{Be}}{\tilde{\tau}}\right)^{1/2} \tag{20}$$

The expression $\phi^3/(1-\phi)$ is an increasing function of ϕ for $0 < \phi < 1$. Therefore, there is no optimal porosity if the length of the heat wheel is optimal. However, there is an optimal porosity if the length is not fixed. The optimal porosity as a function of $\tilde{L}$ may be estimated using the following expression:

$$\phi_{opt} \sim \frac{C}{1+C} \quad \text{where } C \equiv \left(\frac{150\tilde{\rho}\tilde{c}\tilde{L}^2}{\mathrm{Be}\tilde{\tau}}\right)^{1/3} \tag{21}$$

The results presented in this section will be compared to numerical results in the next sections.

4. Numerical optimization: local thermal equilibrium

Eqs. (9) and (12) have been solved numerically with a finite volume approach. Mesh and time step independence were thoroughly tested. The heat transfer rate $\tilde{q}''$ has been calculated first by using 25 control volumes and 25 time steps. The number of control volumes was increased by a factor 2 until the relative difference between heat transfer rates obtained with two consecutive meshing (with respect to their mean value) was smaller than 0.01. For each number of control volumes, the number of time steps has been independently increased by a factor 2 until the same precision was reached for heat transfer rates. It was found that increasing the number of control volumes and time steps above 200 did not change significantly the value of $\tilde{q}''$ for all combination of parameters considered in this paper.

Fig. 2 shows the effect of the heat exchanger length $\tilde{L}$ on the heat transfer rate for three values of the Bejan number for a series of parallel channels. The volumetric heat capacity ratio $\tilde{\rho}\tilde{c}$ retained throughout the paper was 2430 which corresponds to the properties of aluminium and air. As indicated by the scale analysis, there is an optimal value of $\tilde{L}$ that maximizes $\tilde{q}''$. These values are indicated by small white circles in Fig. 2. Also, as expected, $\tilde{L}_{opt}$ increases with the dimensionless pressure drop Be. That is because, for a given period $\tilde{L}_{opt}$, when the available pumping power increases, larger values of $\tilde{L}$ can be considered. The results for non-LTE will be presented and discussed later.

Fig. 3 shows the effect of the porosity φ on the optimal thickness $\tilde{L}_{opt}$ for $\tilde{\tau} = 100$. Each point on this figure is the result of an optimization with respect to $\tilde{L}$. According to Fig. 3, $\tilde{L}_{opt}$ increases drastically with φ and with Be. This result could have been expected since φ is inversely proportional to the internal flow resistance of the RHEx (see Eqs. (3) and (4)) and Be represents the available pumping power. Consequently, the combination of these effects results in a faster flow through the RHEx, which demands for larger values of $\tilde{L}_{opt}$ so that the incoming heated fluid experiences a substantial temperature drop.

Fig. 4 depicts the effect of porosity on the maximized heat transfer rate $\tilde{q}''_m$ (the subscript "m" indicates that all values of $\tilde{q}''$ were maximized with respect to $\tilde{L}$). As shown by our scaling analysis, the optimum porosity is not a function of the pressure drop, and all values of $\tilde{q}''_{mm}$ (see open circles) occur at $\varphi = 0.5$. The

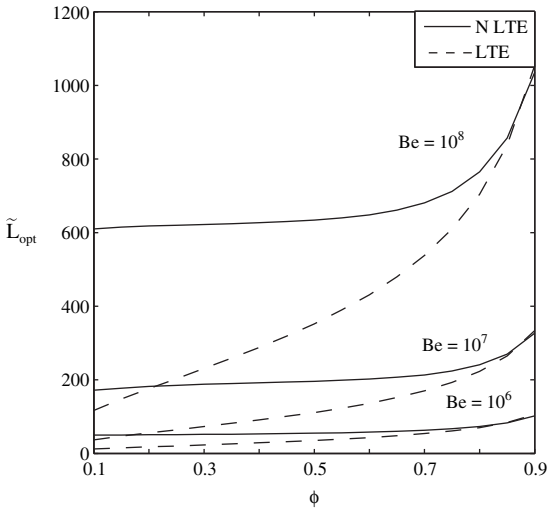

Fig. 3. Optimal length as a function of ϕ and Be (parallel channels).

"mm" subscript indicates that the RHEx has been optimized twice, with respect to φ and $\tilde{L}$.

Figs. 5 and 6 show the variation of $\tilde{q}''_{mm}$ and $\tilde{L}_{opt}$ versus Be and $\tilde{\tau}$. As previously discussed, both variables increase with Be. Moreover, the maximized heat transfer rate $\tilde{q}''_{mm}$ decreases with $\tilde{\tau}$, while $\tilde{L}_{opt}$ increases with this same parameter. Interesting is the fact that the scale analysis was able to capture the relation between the maximized heat transfer rate and optimal RHEx length and the dimensionless pressure drop and half period. This can be seen through the dashed lines in Figs. 5 and 6, which represent a slope of $-1/2$ and $+1/2$, respectively, as revealed by Eq. (19) (i.e., $\tilde{L}_{opt} \sim (\mathrm{Be}\tilde{\tau})^{1/2}$ and $\tilde{q}''_{mm} \sim (\mathrm{Be}/\tilde{\tau})^{1/2}$).

As discussed before, for a packing of spheres, there is no optimal porosity if the length of the wheel has previously been optimized. Since the permeability given by Eq. (5) for a packing of spheres tends towards infinity as φ approaches 1, it will result in large velocities in the RHEx and large optimal length. Therefore, the heat transfer rate will drastically increase with φ. This result is shown in Fig. 7 for $\tilde{\tau} = 100$, where the heat transfer rate $\tilde{q}''_{mm}$ is an increasing

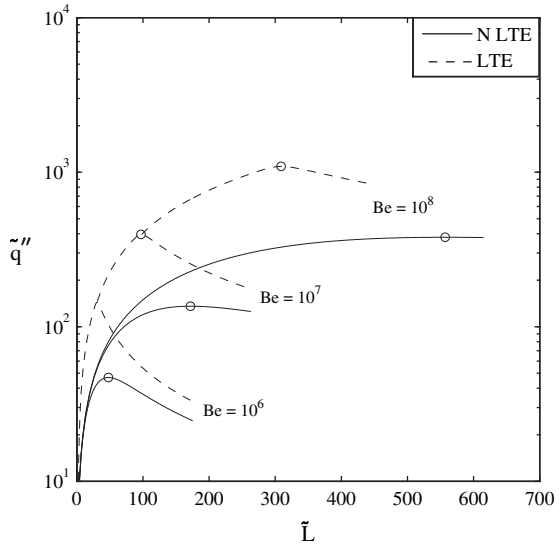

Fig. 2. Heat transfer rate as a function of $\tilde{L}$ and of Be with $\phi = 0.5$ (parallel channels).

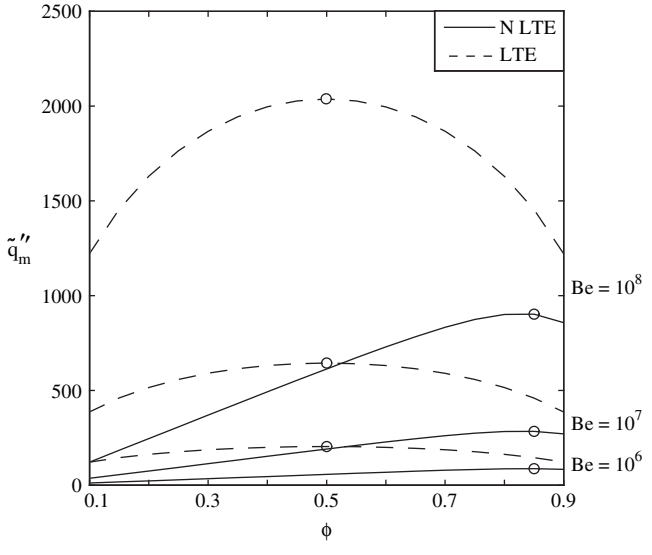

Fig. 4. Heat transfer rate maximized with respect to $\tilde{L}$ as a function of ϕ and Be (parallel channels).

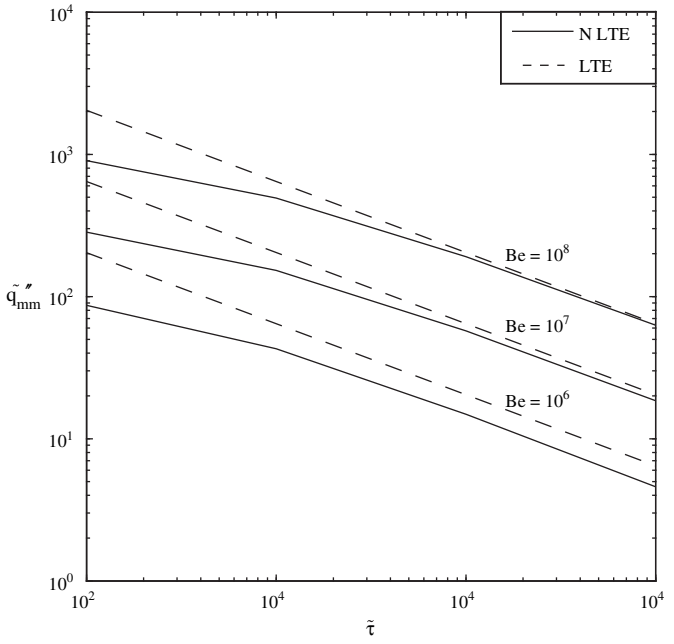

Fig. 5. Heat transfer rate maximized with respect to ϕ and $\tilde{L}$, as a function of $\tilde{\tau}$ and Be (parallel channels).

function of φ. Fig. 8 shows the heat transfer rate $\tilde{q}''_{mm}$ if the length of the wheel is not optimal. On this figure, the dimensionless wheel length $\tilde{L}$ and half period $\tilde{\tau}$ have been set to 100. As predicted by the scale analysis, in that case there is an optimal porosity that maximizes $\tilde{q}''$ indicated by white circles. One can obtain a fair estimate of this optimal porosity with Eq. (21).

5. Two-temperature model

In the previous sections, a simplified model with local thermal equilibrium between the fluid and the solid matrix has been assumed [20,22]. A two-temperature model including conduction will now be used to investigate the effect of non-local thermal equilibrium on both $\tilde{L}_{opt}$ and $\tilde{q}''$ for the two same porous structure

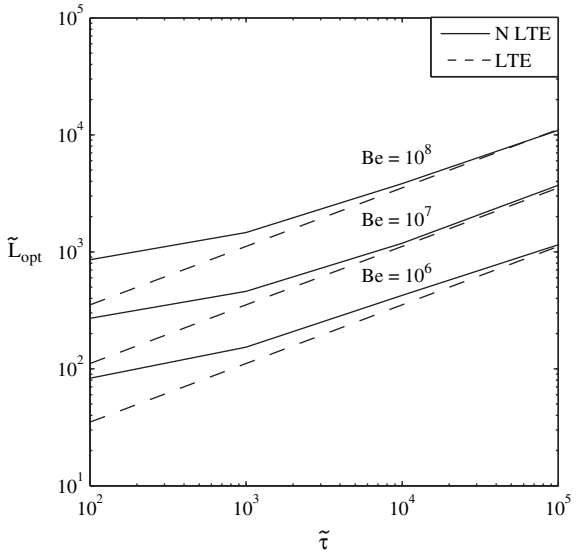

Fig. 6. Optimal length as a function of $\tilde{\tau}$ and Be (parallel channels).

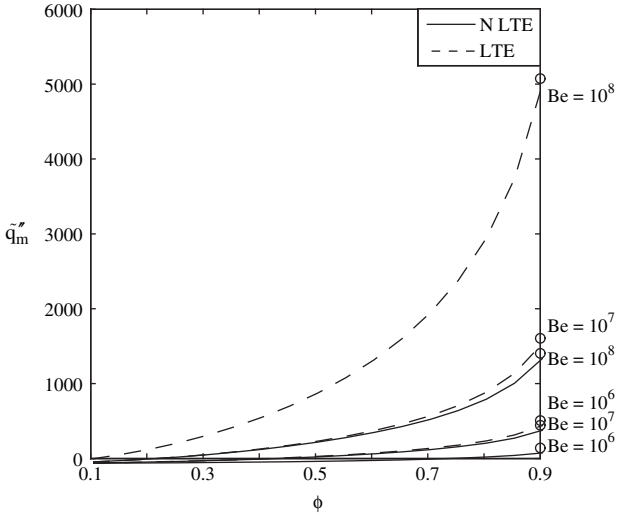

Fig. 7. Heat transfer rate maximized with respect to $\tilde{L}$ as a function of ϕ and Be (packing of spheres).

geometries [21]. The two-temperature model is characterized by the following equations

$$(\rho c)_f\left(\phi\frac{\partial T_f}{\partial t}+u\frac{\partial T_f}{\partial x}\right) = ha\left(T_s-T_f\right) \tag{22}$$

$$(1-\phi)(\rho c)_s\frac{\partial T_s}{\partial t} = (1-\phi)k_s\frac{\partial^2 T_s}{\partial x^2}-ha\left(T_s-T_f\right) \tag{23}$$

The boundary conditions are given by

$$T_f(x=0,0\le t<\tau)=T_H \quad T_f(x=L,\tau\le t<2\tau)=T_C \tag{24}$$

for the fluid and by

$$\frac{\partial T_s(x=0,t)}{\partial x}=0 \quad \frac{\partial T_s(x=L,t)}{\partial x}=0 \tag{25}$$

for the solid matrix. The boundary conditions of Eq. (25) state that heat loss or heat gain from the surroundings is negligible. Heat

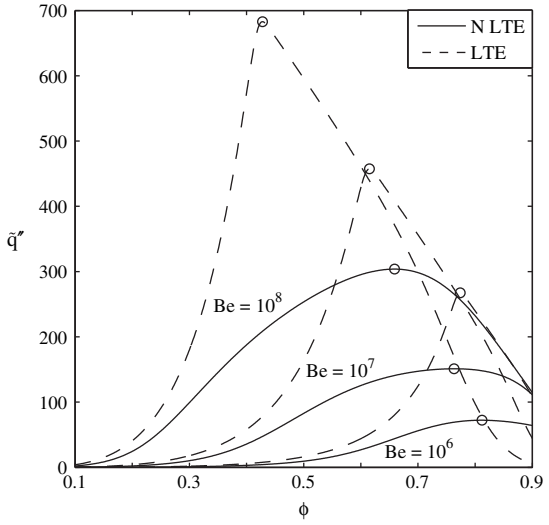

Fig. 8. Heat transfer rate as a function of ϕ and Be when $\tilde{L}$ is not optimized (packing of spheres).

exchange occurs only between the solid matrix and the fluid. The total amount of energy transferred is obtained by applying Eq. (6) to the solid matrix temperature profile.

The constitutive equations were non-dimensionalized using the variables and parameters of Eq. (8) with respect to the fluid properties. The area of heat exchange per unit volume of porous material for a series of parallel channels and a packing of spheres, respectively, may be expressed as [21,24]:

$$a = \frac{4\phi}{D} \quad a = \frac{6(1-\phi)}{D} \tag{26}$$

Eqs. (22) and (23) then become, for a series of parallel channels

$$\phi\frac{\partial\tilde{T}_f}{\partial\tilde{t}} + \frac{\phi}{32}\frac{\mathrm{Be}}{\tilde{L}}\frac{\partial\tilde{T}_f}{\partial\tilde{x}} = 4\phi\mathrm{Nu}\left(\tilde{T}_s - \tilde{T}_f\right) \tag{27}$$

$$(1-\phi)\frac{\rho_s c_s}{\rho_f c_f}\frac{\partial\tilde{T}_s}{\partial\tilde{t}} = (1-\phi)\quad\frac{k_s}{k_f}\frac{\partial^2\tilde{T}_s}{\partial\tilde{x}^2} - 4\phi\mathrm{Nu}\left(\tilde{T}_s - \tilde{T}_f\right) \tag{28}$$

For a packing of spheres, all terms containing $4\phi\mathrm{Nu}(\tilde{T}_s - \tilde{T}_f)$ in Eqs. (27) and (28) are replaced by $6(1-\phi)\mathrm{Nu}(\tilde{T}_s - \tilde{T}_f)$.

The Nusselt number depends on the porous structure. For a series of parallel channels, the Nusselt number may be approximated based on pipe flow correlations. Assuming a fully developed, laminar flow over the entire length of the wheel, the Nusselt number based on the channels diameter D is given by [23]:

$$\mathrm{Nu_D} = 3.66 \tag{29}$$

For a packing of spheres, the Nusselt number, based on an empirical correlation established in [24], may be expressed as

$$\mathrm{Nu}_D = 2 + 1.1\mathrm{Pr}^{1/3}\mathrm{Re}_D^{0.6} = 2 + 1.1\mathrm{Pr}^{15/4}\left(\frac{\tilde{U}}{\tilde{L}}\right)^{0.6} \tag{30}$$

6. Numerical optimization: non-local thermal equilibrium

Equations (27) and (28) have been solved numerically using the finite volume method for both porous structure geometries as described previously. The same criterions have been used for the mesh and time step independence as in Section 4.

Assuming LTE means that the local heat transfer coefficient h is very large. Therefore, both fluid and solid matrix are at the same temperature at the same location in the RHEx. However, the heat transfer coefficient for non-local thermal equilibrium (N-LTE) is finite, which means that the fluid and the solid matrix are not locally at the same temperature. This results in a smaller heat transfer rate between the fluid and the solid. Consequently, in order to achieve its optimal heat transfer rate, the RHEx needs more heat exchange surface. For a given porosity, the optimal wheel length $\tilde{L}_{opt}$ is longer when N-LTE is assumed, as shown in Figs. 2 and 3 for a series of parallel channels. This result remains true for a packing of spheres.

As depicted in Fig. 4 for a series of parallel channels, the maximized heat transfer rate $\tilde{q}''_{mm}$ is smaller for N-LTE and increases with the dimensionless pressure drop Be. The optimal porosity $\varphi_{opt} = 0.85$, indicated by white circles, is greater for N-LTE and is not a function of Be. This result, which is different from that obtained when LTE was assumed, occurs because neither of the conditions of validity for LTE are respected in the studied case. For LTE to be valid, either the non-dimensional length of the wheel $\tilde{L}$ or period 2τ must be very large. The two preceding conditions still depend on Eq. (13), which requires the residence time of the fluid within the wheel to be smaller than the period. A special care should also be taken when φ tends towards 1, since the two-temperature model gives the same results as the one-temperature model. Therefore, the two-temperature model is not valid when $\phi \sim 1$.

As discussed for a series of parallel channels, the maximized heat transfer rate $\tilde{q}''_{mm}$ is smaller if N-LTE is assumed for a packing of spheres (see Fig. 7). Again, there is no optimal porosity if the wheel length is optimal, for the same reasons as for LTE. There is, however, an optimal porosity for N-LTE if $\tilde{L}$ is not optimal, as illustrated in Fig. 8. As expected, this optimal porosity is greater for N-LTE.

7. Porosity distribution

An interesting question that arises is whether it could be beneficial to distribute the solid material differently within the RHEx [20–22,26,27]. An example of porosity distribution is given below:

$$\phi\left(\tilde{x}\right) = A\left\{1 - 4B\left[\frac{\tilde{x}}{\tilde{L}} - \frac{1}{2}\right]^2\right\} \tag{31}$$

This porosity is maximal at the center of the wheel and decreases gradually towards the extremities. Therefore two shape parameters can be varied and optimized, i.e., A and B. Because $0 < \varphi < 1$, we have that $0 < A < 1$ and $0 < B < 1$. To illustrate this optimization opportunity, we considered the parallel channels model.

As the fluid flows through the RHEx, its temperature difference with the solid material diminishes, which results in a decrease of the local heat transfer rate. In order to achieve higher heat transfer rates, the heat exchange area per unit volume must increase. As given by Eq. (26), the heat exchange area per unit volume in an increasing function of φ. Consequently, it could be expected that the porosity near the center of the wheel to be higher than the one near its edges. Moreover, a symmetrical porosity distribution could be expected since fluids enter the RHEx from both ends. As the porosity increases, the heat storage capacity of the RHEx decreases, which, in turn, tends to diminish the maximum heat transfer rate. This competition between heat storage capacity and heat exchange area per unit volume is what explain the existence of an optimal porosity distribution.

Fig. 9a shows the heat transfer rate $\tilde{q}''$ for a series of parallel channels in LTE as a function of both shape parameters A and B. $\tilde{\tau}$ and $\tilde{L}$ were set to 100 and 35. This length was the optimal length found in Section 4, where ϕ was a constant. It can be seen that when ϕ is constant (i.e., when $B = 0$), the optimal porosity is $\phi = 0.5$, as found in Section 4. However, for this length, increasing the porosity at the center of the wheel, while decreasing it near its extremities, results in a higher heat transfer rate, as expected.

Next we optimized simultaneously A, B and $\tilde{L}$. The optimal length for a porosity distribution given by Eq. (31) in LTE with $\mathrm{Be} = 10^6$ is $\tilde{L} = 60$, which is almost twice the optimal length found when ϕ was constant. Fig. 9b depicts the heat transfer rate as a function of A and B for this length. By comparing Fig. 9a and b, it can be seen that the maximal heat transfer rate is almost twice as large when the porosity is not a constant, but a distribution given by Eq. (31). The optimal porosity distribution is found to be independent of the Bejan number (as when the porosity was constant) and the optimal parameters are $A = 0.95$ and $B = 0.80$, which gives a mean porosity of $\bar{\phi} \sim 0.7$. This porosity distribution is illustrated in Fig. 10.

The same three parameters were optimized for NLTE. As for LTE, there exist two distinct maxima: one when ϕ is a constant ($B = 0$)

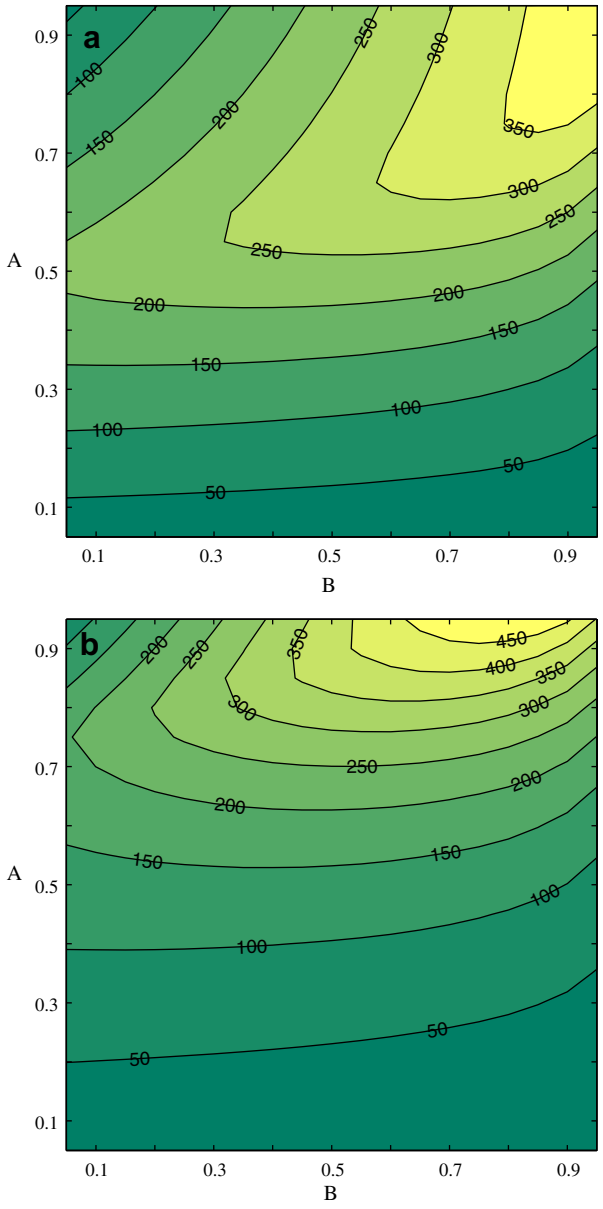

Fig. 9. Optimal values of A and B (porosity distribution) for: a) optimized length when ϕ was uniform, and b) optimized length with ϕ from Eq. (31).

and one when ϕ is a function of both A and B. However, for NLTE, the heat transfer rates corresponding to each of the two maxima are very close. It was found that when $\mathrm{Be} \lesssim 3\times10^6$, the optimal porosity distribution is $A=0.95$ and $B=0.85$. Optimal lengths for this distribution are relatively small. For example, $\tilde{L}_{\mathrm{opt}} = 46$ and 54 for $\mathrm{Be}=1\times10^6$ and 2×10^6, respectively. When $\mathrm{Be} \gtrsim 3\times10^6$, the heat transfer rate of the ($\phi=$ constant) maximum becomes higher than that when ϕ is a function of A and B. The optimal porosity is then given by $A=0.85$ and $B=0$, which is the same optimal porosity as the one found in Section 6. Optimal lengths when ϕ is a constant are much larger than those when ϕ was not constant. When $\mathrm{Be}=4\times10^6$, the optimal length $\tilde{L}_{\mathrm{opt}} = 163$, which is three times larger than the one found for $\mathrm{Be}=2\times10^6$. This means that there are two optimal RHEx configurations: low Be with short wheel and the porosity distribution of Eq. (31), or high Be with long wheel and a constant porosity. Independently, the maximal heat transfer rate increases with Be.

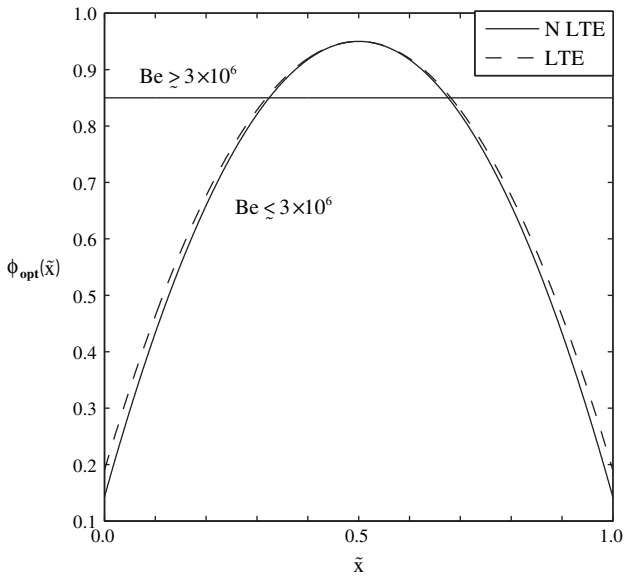

Fig. 10. Optimal porosity distribution (parallel channels).

8. Imbalance between the hot and cold flows

In the previous sections, the hot and cold fluid streams were presumed to be both injected within the RHEx during half of the period of rotation of the wheel. Since both hot and cold fluids had the same heat capacity rates, the heat transferred from fluid to solid matrix was the same for the first and the second half period. This corresponds to a RHEx for which 50% of the surface area is occupied by the hot fluid, and 50% by the cold fluid. In other words, the optimal angle ratio $\theta_{\mathrm{H,opt}}/\theta_{\mathrm{C,opt}}$ was presumed to be 1, where θ_{H} and θ_{C} are the angles of the wheel in which hot and cold fluids are injected, respectively (see Fig. 1). However, it is reasonable to assume that the optimal angle ratio $\theta_{\mathrm{H,opt}}/\theta_{\mathrm{C,opt}}$ will not be 1 if the hot and cold fluids heat capacity rates differ. In this section, we determine the optimal angle ratio when the hot and cold fluids are driven by different Bejan numbers $\mathrm{Be_H}$ and $\mathrm{Be_C}$.

Similarly to the scale analysis developed in Section 3, it is possible to estimate the optimal length of the RHEx as a function of $\mathrm{Be_C}$ and $\mathrm{Be_H}$ for LTE. The optimal heat exchanger length is such that the length thermally influenced during the hot fluid injection time t_{H} scales as $\tilde{L}$ in such a way that all the domain is properly used. The same is true for t_{C}, the time during which cold fluid is injected within the wheel. From Eq. (1), it is possible to find the order of magnitude of each time t_{H} and t_{C}:

$$t_{\mathrm{H}} \sim \frac{\sigma L}{u_{\mathrm{H}}} \quad \text{and} \quad t_{\mathrm{C}} \sim \frac{\sigma L}{u_{\mathrm{C}}} \tag{32}$$

Using the fact that $t_{\mathrm{H}} + t_{\mathrm{C}} = 2\tau$ with Eqs. (3), (4), and (8) for a series of parallel channels and assuming $\sigma \sim (1-\phi)\tilde{\rho}\tilde{c}$ (since $\tilde{\rho}\tilde{c} \gg 1$), the following result is obtained:

$$\tilde{L}_{\mathrm{opt}} \sim \left(\frac{\phi}{16(1-\phi)\tilde{\rho}\tilde{c}} \frac{\mathrm{Be_H}\tilde{\tau}}{(1+\mathrm{Be_H}/\mathrm{Be_C})} \right)^{1/2} \tag{33}$$

When $\mathrm{Be_C} = \mathrm{Be_H} = \mathrm{Be}$, Eq. (33) becomes Eq. (18). From Eq. (32), since u_{H} is directly proportional to $\mathrm{Be_H}$ and u_{C} is directly proportional to $\mathrm{Be_C}$, the following relations is obtained:

$$\frac{t_{\mathrm{H,opt}}}{t_{\mathrm{C,opt}}} \sim \frac{\mathrm{Be_C}}{\mathrm{Be_H}} \quad \text{or} \quad \frac{\theta_{\mathrm{H,opt}}}{\theta_{\mathrm{C,opt}}} \sim \frac{\mathrm{Be_C}}{\mathrm{Be_H}} \tag{34}$$

Simulations were performed for a series of parallel channels to obtain $\theta_{H,opt}/\theta_{C,opt}$ as a function of Be_C/Be_H. Bejan number ratios ranged from 1 to 10, where Be_H was set to 10^6. Since the heat capacity rate is proportional to the velocity, and the velocity is directly proportional to Be for a series of parallel channels, using different Be_H and Be_C is the same as using different heat capacity rates. As found in Sections 4 and 6, the optimal porosity, when ϕ is constant, is not a function of the dimensionless pressure drop Be. Therefore, simulations were carried with $\phi_{opt} = 0.5$ for LTE and $\phi_{opt} = 0.85$ for NLTE, with a dimensionless half period $\tilde{\tau} = 100$. Note that simulations were performed with other $\tilde{\tau}$-values, but results were exactly the same. In other words, the optimal ratio $\theta_{H,opt}/\theta_{C,opt}$ is not a function of the period. For each ratios Be_C/Be_H and θ_H/θ_C, the length of the wheel has been optimized in order to maximize the heat transfer rate.

The optimal angle ratio is reported in Fig. 11 as a function of the flow imbalance, Be_C/Be_H. The following correlations were obtained for LTE and NLTE respectively, with a maximal error of 3% for Eq. (35) and 11% for Eq. (36):

$$\theta_{H,opt}/\theta_{C,opt} = 1.0216(Be_C/Be_H)^{0.8958} \quad \text{where} \quad 1 \times < \frac{Be_C}{Be_H} < 10 \quad \text{(LTE)} \tag{35}$$

$$\theta_{H,opt}/\theta_{C,opt} = 1.0838(Be_C/Be_H)^{0.6837} \quad \text{where} \quad 1 \times < \frac{Be_C}{Be_H} < 10 \quad \text{(NLTE)} \tag{36}$$

These correlations are independent on $\tilde{\tau}$ and they are close to the relation obtained from scale analysis (Eq. (34)).

Also, we report here the optimal length in the presence of flow imbalance. Correlations for the optimal length of the wheel are given below for LTE and NLTE, with a maximal error of 2% for Eq. (37) and 1% for Eq. (38), and for a dimensionless half period $\tilde{\tau} = 1000$:

$$\tilde{L}_{opt} = \frac{96.047}{(1 + Be_C/Be_H)} + 64.238 \quad \text{where} \quad 1 < \frac{Be_C}{Be_H} < 10 \quad \text{(LTE)} \tag{37}$$

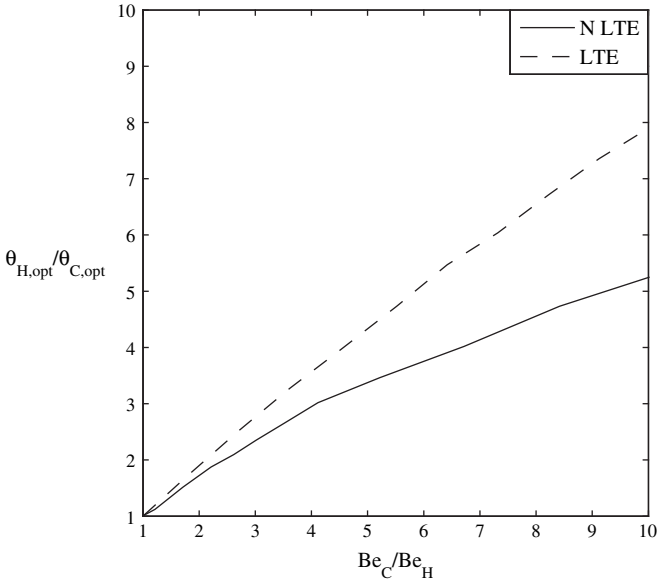

Fig. 11. Optimal angle ratio as a function of the flow imbalance.

$$\tilde{L}_{opt} = \frac{238.8}{(1 + Be_C/Be_H)} + 130.67 \quad \text{where} \quad 1 \times < \frac{Be_C}{Be_H} < 10 \quad \text{(NLTE)} \tag{38}$$

These results agree satisfactorily with the scale analysis prediction (Eq. (33)).

9. Conclusions

In the present paper, we showed that the performance of a rotary heat exchanger could be drastically improved by properly selecting its thickness (i.e., length L) and the porosity of the internal thermal mass. More specifically, the numerical results show that $\varphi_{opt} = 0.5$ and 0.85 for the LTE and N-LTE models, respectively, regardless of the dimensionless pressure drop (Be), while L_{opt} is strongly affected by Be (See Fig. 3).

As expected, the numerical predictions also reveal that the efficiency of RHEx under idealized thermal equilibrium (LTE) conditions is higher than the maximized performances obtained with the non-local thermal equilibrium (N-LTE) model. That is due to the high heat transfer coefficient indirectly imposed between the solid matrix under the LTE approach (Section 6). Furthermore, the performance of the RHEx was nearly doubled by allowing the porosity of the porous matrix to be unevenly distributed over the length L (Section 7). In this case, a quadratic function was used for the porosity $\varphi(x)$. The function was specifically tailored in a way to present a maximum value at $x/L = 0.5$, and identical minimum values at $x/L = 0$ and 1 as discussed in Section 7.

Finally, the study ends by considering the effect of the relative period for the heating and cooling streams acting on the RHEx. This was shown to be equivalent to RHEx thermally connecting two streams of different heat capacities. The numerical results, which were validated with scaling analysis, show that the flow with the highest heat capacity rate should occupy a smaller frontal area (i.e., should stay in contact with the solid matrix for a shorter period than the low heat capacity rate fluid). Correlations between the period and the dimensionless pressure drop of each stream were proposed.

Future studies may extend the present work by including 2-D or 3-D effects as well as fouling, frosting and leakage, since these are realistic issues addressed by the specialized community. Furthermore, one can envision to design in detail the internal structure of the porous core leading to a designed porous medium with non-uniform distributions [20–22,26–28].

Acknowledgements

L. Gosselin's work is supported by the Natural Sciences and Engineering Research Council of Canada (NSERC).

References

[1] R.K. Shah, D.P. Sekulic, Fundamentals of Heat Exchanger Design, John Wiley & Sons, Inc., New York, 2003.
[2] F.P. Incropera, D.P. Dewitt, T.L. Bergman, A.S. Lavine, Fundamentals of Heat and Mass Transfer, John Wiley & Sons, Inc., New York, 2007.
[3] C.F. Bonilla, Thermowheel rotary air-to-air heat-exchanger – engineering characteristics and economics, Archives of Environmental Health 4 (1962) 285–294.
[4] D. Goricanec, J. Krope, The economic-advantages of using a rotary heat regenerator, Strojniski Vestnik. (Journal of Mechanical Engineering) 40 (1994) 115–122.
[5] R.K. Jassim, Evaluation of combined heat and mass transfer effect on the thermoeconomic optimization of an air-conditioning rotary regenerator, Journal of Heat Transfer – Transactions of the ASME 125 (2003) 724–733.

[6] T. Skiepko, The effect of matrix longitudinal heat-conduction on the temperature-fields in the rotary heat-exchanger, International Journal of Heat and Mass Transfer 31 (1988) 2227–2238.
[7] J.Y. San, S.C. Hsiau, Effect of axial solid heat-conduction and mass diffusion in a rotary heat and mass regenerator, International Journal of Heat and Mass Transfer 36 (1993) 2051–2059.
[8] S. Nair, S. Verma, S.C. Dhingra, Rotary heat exchanger performance with axial heat dispersion, International Journal of Heat and Mass Transfer 41 (1998) 2857–2864.
[9] M. Porowski, E. Szczechowiak, Influence of longitudinal conduction in the matrix on effectiveness of rotary heat regenerator used in air-conditioning, Heat and Mass Transfer 43 (2007) 1185–1200.
[10] M. Younis, M. Shoukry, Regenerative rotary heat-exchanger for heat-recovery in residential ventilation, International Journal of Energy Research 7 (1983) 315–325.
[11] R.G. Whitbeck, K.H. Hemsath, A. Prasad, High-temperature heat wheel for industrial heat-recovery, American Ceramic Society Bulletin 63 (1984) 1015–1015.
[12] Z. Wu, R.V.N. Melnik, F. Borup, Model-based analysis and simulation of regenerative heat wheel, Energy and Buildings 38 (2006) 502–514.
[13] O. Buyukalaca, T. Yilmaz, Influence of rotational speed on effectiveness of rotary-type heat exchanger, Heat and Mass Transfer 38 (2002) 441–447.
[14] T. Skiepko, Method of monitoring and measuring seal clearances in a rotary heat-exchanger, Heat Recovery Systems and CHP 8 (1988) 469–473.
[15] T. Skiepko, Effect of reduction in seal clearances on leakages in a rotary heat-exchanger, Heat Recovery Systems and CHP 9 (1989) 553–559.
[16] B. Frankovic, Heat-transfer analysis in dry rotary heat-exchanger, Strojarstvo 35 (1993) 111–120.
[17] C.J. Simonson, R.W. Besant, Energy wheel effectiveness: part i – development of dimensionless groups, International Journal of Heat and Mass Transfer 42 (1999) 2161–2170.
[18] C.J. Simonson, R.W. Besant, Energy wheel effectiveness: part ii – correlations, International Journal of Heat and Mass Transfer 42 (1999) 2171–2185.
[19] E.M. Sparrow, J.C.K. Tong, M.R. Johnson, G.P. Martin, Heat and mass transfer characteristics of a rotating regenerative total energy wheel, International Journal of Heat and Mass Transfer 50 (2007) 1631–1636.
[20] P. Wildi-Tremblay, L. Gosselin, Layered porous media architecture for maximal cooling, International Journal of Heat and Mass Transfer 50 (2007) 464–478.
[21] G. Leblond, L. Gosselin, Effect of non-local equilibrium on minimal thermal resistance porous layered systems, International Journal of Heat and Fluid Flow 29 (2008) 281–291.
[22] M. Tye-Gingras, L. Gosselin, Thermal resistance minimization of a fin-and-porous-medium heat sink with evolutionary algorithms, Numerical Heat Transfer Part A: Applications 54 (2008) 349–366.
[23] A. Bejan, Convection Heat Transfer, John Wiley & Sons, Inc., New York, 2004.
[24] A. Amiri, K. Vafai, Analysis of dispersion effects and nonthermal equilibrium, non-Darcian, variable porosity incompressible-flow through porous-media, International Journal of Heat and Mass Transfer 37 (1994) 939–954.
[25] A. Bejan, Shape and Structure: From Engineering to Nature, Cambridge University Press, Cambridge, 2000.
[26] A. Bejan, Designed porous media: maximal heat transfer density at decreasing length scales, International Journal of Heat and Mass Transfer 47 (2004) 3073–3083.
[27] J.C. Ordonez, A. Bejan, R.S. Cherry, Designed porous media: optimally nonuniform flow structures connecting one point with more points, International Journal of Thermal Sciences 42 (2003) 857–870.
[28] A.K. da Silva, G. Lorenzini, A. Bejan, Distribution of heat sources in vertical open channels with natural convection, International Journal of Heat and Mass Transfer 48 (2005) 1462–1469.